A Simple Monte Carlo Transport and Multiplication Simulation Method for the Analysis of a SPAD with a Spherically Uniform Electric Field Peak

Edward Van Sieleghem[1,2,4], Andreas Süss[2,3], Gauri Karve[2],
Koen De Munck[2], Chris Van Hoof[1,2], Jiwon Lee[2]
[1]*KU Leuven, ESAT, Kasteelpark Arenberg 10, 3001 Leuven, Belgium*
[2]*Imec, Kapeldreef 75, 3001 Leuven, Belgium*
[3]*now at OmniVision Technologies, Santa Clara CA 95054, USA*
[4]*Corresponding author, email: edward.vansieleghem@imec.be*

***Abstract*—A Monte Carlo simulation method for the transport and multiplication of carriers in electric fields is presented. The method is based on the stochastic scattering and free flight of electrons and holes in silicon. The simulation technique employs a nonparabolic single-band model for the energy dispersion relation, providing good accuracy for high electric fields while keeping the complexity of the simulator low. Phonon scattering and impact ionization scattering are considered. The tool is used to estimate the photon detection efficiency, temporal response, noise, and crosstalk of a near-infrared enhanced single-photon avalanche diode (SPAD) with a spherically uniform electric field peak. Since the field is not laterally uniform, methods that do not consider the stochastic dynamics of individual carriers prove inaccurate. Good agreement is found between measurements and Monte Carlo simulation results of the device, indicating that the tool is useful for the ab initio design and optimization of SPADs.**

I. Introduction

Single-photon avalanche diodes (SPADs) can resolve individual photons with high temporal accuracy by exploiting the avalanche breakdown phenomenon in the electric fields of semiconductor junctions. Prominent application domains of SPADs are biophotonics [1] and time-of-flight (ToF) imaging [2]. In particular, ToF depth-sensing based on SPADs is gaining increased interest from the automotive and mobile industries [3]. This application requires a high near-infrared (NIR) sensitivity and benefits from SPADs fabricated in well-established silicon integration technologies.

Numerical and analytical modeling techniques aid in the design and analysis of SPADs. The performance of these detectors, including the photon detection efficiency (PDE), temporal response, and dark count rate (DCR), can be estimated from the electric fields and carrier generation profiles extracted by numerical tools. Some modeling techniques employ deterministic calculations along one-dimensional electric field lines in the device [4]. These methods typically make abstraction of the stochastic dynamics of individual charge carriers, and are less accurate for SPADs with nonuniform or steep junction profiles. Alternatively, by considering the stochastic transport and avalanche multiplication behavior of single carriers, more accurate analysis results and physical insight can be obtained, even for devices with steep and nonuniform electric fields [5].

This work was supported in part by Research Foundation – Flanders (FWO) SB PhD fellowship under Grant 11D3321N.

The Monte Carlo method allows for simulating the random movement and multiplication of carriers. Statistical conclusions are drawn about the behavior of a SPAD by stochastically simulating the dynamics of a large sample of individual carriers in the device [6]. Avalanche multiplication is a cyclic infinite-gain impact ionization process between electrons and holes. Therefore, Monte Carlo simulators for SPADs must consider both carrier types.

From a semi-classical perspective, a charge carrier is a quasi-particle with energy E and wavevector $\mathbf{k}$. Electrons and holes occupy discrete energy levels defined by the dispersion relation $E(\mathbf{k})$. This relation consists of many bands with allowed states in k-space. Carriers hop between states under the influence of electric fields (free flight) and because of random scattering events. Simulation of the carrier dynamics requires the modeling of $E(\mathbf{k})$ and the scattering mechanisms. Full-band Monte Carlo methods include full, physically accurate, models of the dispersion relation and scattering mechanisms [7]. These methods are difficult to calibrate and slow in execution. However, the simulation results are accurate for most devices and junction profiles. Alternatively, single-band Monte Carlo methods simplify the dispersion relation by considering a single energy band for each carrier type [8]. These methods are fast and simple. However, to the knowledge of the authors, existing single-band techniques for SPADs employ parabolic energy dispersion relations which are less accurate for hot carriers in high electric fields.

In this work, we propose a single-band Monte Carlo simulation method based on a nonparabolic isotropic dispersion relation for electrons and holes in depleted intrinsic silicon. The method considers phonon scattering [6] and impact ionization scattering [8]. The technique is used to analyze a frontside illuminated (FSI) NIR-enhanced silicon SPAD with a spherically uniform electric field peak [9]. Due to the nonuniform field, the performance is difficult to extract with deterministic techniques.

II. Monte Carlo Method

The dispersion relation defines the allowed energy states between which carriers can move freely and scatter. At low energies, the $E(\mathbf{k})$ relation is approximately parabolic. When carriers gain sufficient energy under the influence of high fields, the parabolic approximation breaks down. To capture high energy phenomena, this work employs a nonparabolic isotropic dispersion relation

$$E(\mathbf{k})(1+\rho E(\mathbf{k})) = \frac{\hbar^2\mathbf{k}^2}{2m^*},$$

with non-parabolicity factor ρ and effective carrier mass m^* [6]. The conduction band for electrons and the valence band for holes are modeled by the same equation, but with different parameter values.

The main scattering mechanisms in depleted intrinsic silicon are phonon absorption, phonon emission, and impact ionization [6]. The average phonon energy in silicon is $\hbar\omega \approx 63$ meV, with reduced Planck constant $\hbar$ and phonon frequency ω [8]. The phonon occupation factor N_{ph} at temperature T equals $\left[\exp\left(\hbar\omega/k_{\mathrm{b}}T\right)-1\right]^{-1}$, with Boltzmann constant k_{b}.

During phonon absorption events, the carrier energy increases from E to $E_{\mathrm{ab}} = E + \hbar\omega$. The scattering process isotropically randomizes the wavevector while ensuring that $E(\mathbf{k})$ is satisfied. The phonon absorption scattering rate is proportional to the product of the phonon density and the carrier density-of-states ($\propto \mathbf{k}^2\,\mathrm{d}\mathbf{k}/\,\mathrm{d}E$ [6]) after scattering, and it is given by

$$S_{\mathrm{ab}} = \begin{cases} C_{\mathrm{ph}}N_{\mathrm{ph}}(1+2\rho E_{\mathrm{ab}}) \\ \qquad\qquad \times\sqrt{E_{\mathrm{ab}}(1+\rho E_{\mathrm{ab}})} & \text{if} E \geq 0 \\ 0 & \text{otherwise} \end{cases},$$

with fitting parameter C_{ph}. The value of C_{ph} depends on the carrier type. Phonon emission is modeled analogously to phonon absorption [6]. During emission events, the carrier energy decreases from E to $E_{\mathrm{em}} = E - \hbar\omega$, and the wavevector changes randomly. The phonon emission rate equals

$$S_{\mathrm{em}} = \begin{cases} C_{\mathrm{ph}}(N_{\mathrm{ph}}+1)(1+2\rho E_{\mathrm{em}}) \\ \qquad\qquad \times\sqrt{E_{\mathrm{em}}(1+\rho E_{\mathrm{em}})} & \text{if} E \geq \hbar\omega \\ 0 & \text{otherwise} \end{cases}.$$

Impact ionization scattering occurs when a primary carrier gains sufficient energy to excite a new secondary electron-hole pair. The ionization scattering rate is empirically modeled by the Keldysh formula

$$S_{\mathrm{ii}} = \begin{cases} C_{\mathrm{ii}}\left(\frac{E-E_{\mathrm{th}}}{E_{\mathrm{th}}}\right)^{\delta} & \text{if} E \geq E_{\mathrm{th}} \\ 0 & \text{otherwise} \end{cases},$$

with ionization prefactor C_{ii}, threshold energy E_{th}, and softness factor δ [8]. The initial energy E of the primary carrier splits over the three involved charges. The final energy of each charge equals $E_{\mathrm{ii}} = (E - E_{\mathrm{th}})/3$. Additionally, the wavevectors of the carriers are isotropically randomized.

Fig. 1 presents a stochastic Monte Carlo simulation flow for the transport and multiplication of carriers in the electric field of a SPAD. Each simulation trial starts from a single charge at an arbitrary point of generation. The free flight and scattering of the carrier are simulated iteratively by using the self-scattering principle [6]. Whenever impact ionization occurs, the newly generated electron and hole are traced independently. Herein, carrier-carrier interactions are not considered. The simulation stops when all carriers have arrived at a device electrode or when the total number of ionization events exceeds the threshold value N_{max}. The threshold condition signifies the occurrence of avalanche breakdown. The simulation outputs the number of carriers arriving at each electrode versus time (the instantaneous current) and the total simulated time. By combining simulation results for many individually generated carriers, statistical conclusions are drawn about the SPAD's performance.

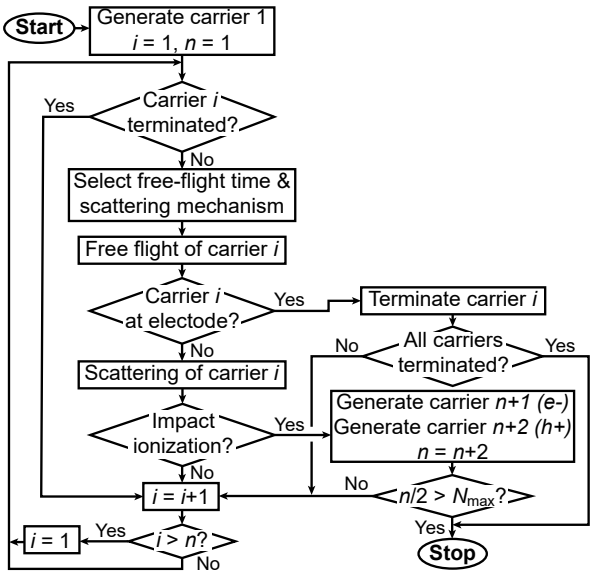

Fig. 1. Stochastic simulation flow for the transport and multiplication of carriers in the field of a SPAD, starting from a single generated carrier.

Table I presents the simulator parameters in silicon at room temperature. The ionization parameter values are taken from reference [8]. The other parameters are calibrated to provide a good match with empirical models for the carrier velocity [10] and ionization rates [11]. Fig. 2 presents a comparison between the nonparabolic single-band technique of this work, a parabolic single-band method by Zhou et al. [8], and the empirical models. The nonparabolic technique captures high field phenomena such as velocity saturation and impact ionization with higher accuracy.

III. SPAD Analysis and Discussion

The Monte Carlo technique enables the investigation of SPAD behavior. Performance estimations are made based on the stochastic transport and avalanche multiplication probability of a random sample of carriers generated according to a simulated spatial distribution. In this work, only carriers generated by light are considered.

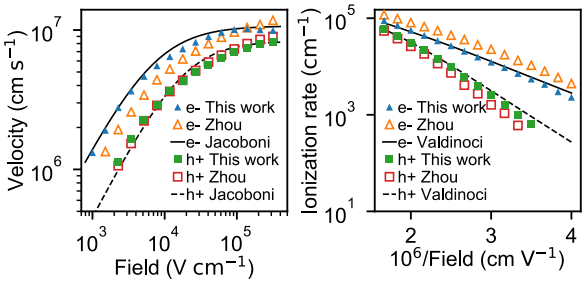

Fig. 2. Carrier velocity and ionization rates of electrons (e-) and holes (h+) in silicon obtained by the presented method (This work), a parabolic technique (Zhou [8]), and empirical models (Jacoboni [10] and Valdinoci [11]).

TABLE I
MONTE CARLO MODEL PARAMETERS IN SILICON

	Electron	Hole
Effective mass m^* (kg)	$0.57m_0$[†]	$1.07m_0$[†]
Non-parabolicity factor ρ (eV^{-1})	0.13	0.02
Phonon energy $\hbar\omega$ (meV)	63	63
Phonon prefactor C_{ph} (Hz/$\sqrt{\mathrm{eV}}$)	$1 \cdot 10^{23}$	$1.5 \cdot 10^{23}$
Ionization prefactor C_{ii} (Hz)	$2 \cdot 10^{12}$	$4.4 \cdot 10^{12}$
Ionization softness δ	3.5	3.5
Ionization threshold E_{th} (eV)	1.2	1.5

[†]Free electron mass m_0

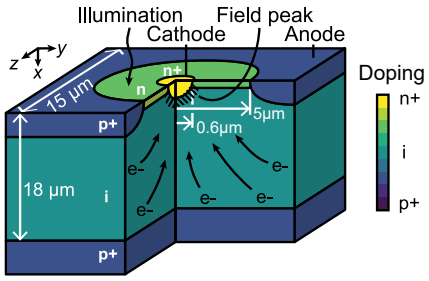

Fig. 3. Doping schematic of a NIR enhanced SPAD (Adapted from [9]). Electrons (e-) generated in the absorption region drift towards a field peak.

The method is applied to the NIR enhanced FSI silicon SPAD presented in Fig. 3 [9]. The device contains a depleted absorption volume of 15 µm × 15 µm × 18 µm on top of a p-type substrate. The electrons generated in the absorption volume drift to an active region with a diameter of ≈ 1.5 µm in which they have a high probability of triggering avalanche breakdown. The active region is cylindrically symmetric and contains a spherically uniform electric field peak enforced by field-line crowding. The absorption and multiplication volumes are mainly situated in depleted and lowly-doped regions, justifying the use of the simple Monte Carlo simulation technique. To reduce complexity, the charge carrier behavior in the active region and absorption volume are simulated separately.

Firstly, the breakdown probability of electrons entering the active region is extracted. To this end, the transport and multiplication (impact ionization) of a sample of electrons entering the active region at collection angle α_{c} and radius $r_{\mathrm{c}} = 1.5$ µm is simulated

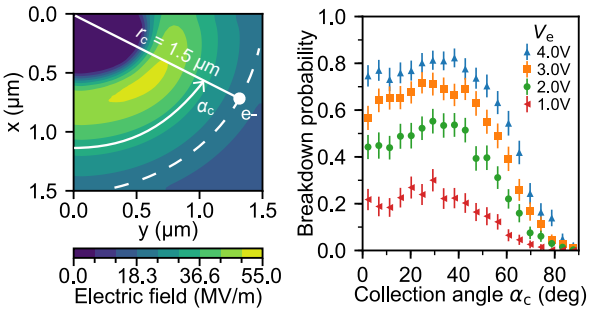

Fig. 4. Left: Simulated electric field near the cathode ($V_{\mathrm{e}} = 3.5$ V; top interface $x = 0$ µm; centerline $y = 0$ µm). Right: Breakdown probability for electrons entering the active region at radius $r_{\mathrm{c}} = 1.5$ µm and angle α_{c} (with 95% confidence intervals).

(breakdown threshold $N_{\max} = 1000$, sample size 9000). Fig. 4 illustrates the field in the active region for excess bias $V_{\mathrm{e}} = 3.5$ V. Additionally, the plot on the right demonstrates the breakdown probability versus α_{c} for different values of V_{e}. The probability is low for electrons generated near the top interface (with large α_{c}) and high for electrons generated at larger depths (with small α_{c}).

Secondly, the transport statistics of carriers are determined. To this end, the movement of a random sample of electrons is simulated in the absorption volume while impact ionization is disabled (sample size 21000). The contribution of each electron to the SPAD performance estimates is weighted by two factors: (a) the generation rate at its point of origin $(x_{\mathrm{g}}, y_{\mathrm{g}})$ and (b) the breakdown probability for the angle α_{c} at which it enters the active region (Fig. 4). In the following, an excess bias of 3.5 V is considered.

The **photon detection efficiency** is estimated based on numerically simulated optical generation profiles. Fig. 5 illustrates the optical simulation domain and the generation profile for wavelength $\lambda = 900$ nm. The back end of the device contains dummy metal regions that reflect approximately half of the incident light and serve no functional purpose [9]. Fig. 6(a) demonstrates the simulated and measured PDE, which overlap significantly. The qualitative difference can be attributed to optical interference and modeling inaccuracies. In particular, the light source in the simulation is monochromatic and collimated. These conditions are not fully satisfied for the measurement [9]. The PDE at visible wavelengths is reduced because of the low breakdown probability of shallowly generated carriers.

The **temporal response** resembles the uncertainty in the timing of individual incident photons. The response depends on the variability of the transport, multiplication, and readout processes of photons absorbed in the device. Fig. 6(b) presents the measured temporal response of the investigated SPAD at $\lambda = 905$ nm (full width at half maximum ≈ 350 ps), which is obtained by binning the time-difference between picosecond-laser pulses and breakdown events. The curve is shifted to 0 ns for clarity. The figure also includes the histogram of the transport time for photo-generated

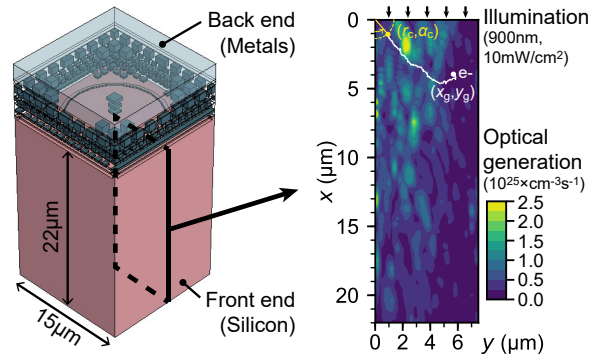

Fig. 5. Left: Electromagnetic-wave simulation domain with (dummy) metal layers. Right: Optical generation cross-section for $\lambda = 900$ nm, and example of an electron transport trial.

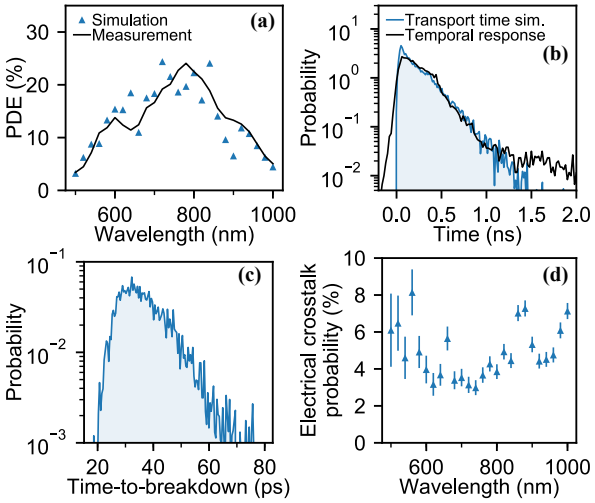

Fig. 6. Results for $V_e = 3.5$ V. (a) Simulated and measured PDE. (b) Simulated transport time distribution and measured temporal response for $\lambda \approx 900$ nm. (c) Simulated time-to-breakdown distribution for $\lambda = 900$ nm. (d) Simulated electrical crosstalk probability with 95% confidence intervals.

electrons at $\lambda = 900$ nm, as simulated by the Monte Carlo method. The measurement and simulation overlap significantly, suggesting that the temporal response is dominated by variability in electron transport. The discrepancy in the tail indicates that not all diffusing carriers are captured by the simulation, most likely, due to the finite depth of the simulation domain. The discrepancy in the peak can be explained by additional timing variance components, for example, due to the multiplication process. Fig. 6(c) presents the simulated histogram for the time between which electrons enter the active region and trigger breakdown (time-to-breakdown). This distribution corresponds to the additional timing uncertainty resulting from charge multiplication.

The **electrical crosstalk** is defined as the fraction of carriers generated in a central SPAD that diffuse to neighboring SPADs before triggering breakdown. Fig. 6(d) presents the simulated electrical crosstalk probability versus λ. The SPAD is isolated from neighbors by small potential barriers resulting in a relatively high electrical crosstalk probability of $\approx$ 5%. The wavelength dependence indicates that the electrical crosstalk probability is a function of the generation depth. Besides, optical crosstalk due to optical generation during breakdown events may be a topic of future research.

Carriers generated by traps on the top interface have large collection angles α_c. Therefore, these dark carriers have low breakdown probabilities (Fig. 4) and small contributions to the **dark count rate**. The measured DCR has an activation energy of 0.88 eV at room temperature [9]. This energy is close to the bandgap, indicating that the DCR contribution from trap-assisted generation is indeed not dominant. Additionally, the absence of traps in the field peak and the small active volume enable an exceptionally low **afterpulsing** probability of $< 0.1\%$ [9]. Qualitative modeling of noise sources based on dark carrier generation is beyond the scope of this work.

IV. Conclusions

A single-band Monte Carlo method is defined and used for analyzing a NIR-enhanced SPAD. The simulation results agree with the measurements and expectations of the fabricated device. Additionally, the Monte Carlo method provides valuable physical insight into the behavior of the detector. Consequently, the tool can be used to design and analyze the doping profiles of SPADs for which existing methods are not sufficiently accurate.

References

[1] C. Bruschini et al., "Single-photon avalanche diode imagers in biophotonics: review and outlook," *Light Sci. Appl.*, vol. 8, art. 87, Sept. 2019.

[2] K. Morimoto et al., "Megapixel time-gated SPAD image sensor for 2D and 3D imaging applications," *Optica*, vol. 7, no. 4, pp. 346–354, 2020.

[3] K. Ito et al., "A back illuminated 10μm SPAD pixel array comprising full trench isolation and Cu-Cu Bonding with over 14% PDE at 940nm," in *Int. Electron Devices Meeting*, pp. 347–350, 2020.

[4] Y. Xu et al., "A new modeling and simulation method for important statistical performance prediction of single photon avalanche diode detectors," *Semicond. Sci. Technol.*, vol. 31, no. 6, art. 065024, 2016.

[5] S. A. Plimmer et al., "A simple model for avalanche multiplication including deadspace effects," *IEEE Trans. Electron Devices*, vol. 46, no. 4, pp. 769–775, 1999.

[6] C. Jacoboni et al., "The Monte Carlo method for the solution of charge transport in semiconductors with applications to covalent materials," *Rev. Mod. Phys.*, vol. 55, no. 3, pp. 645–705, 1983.

[7] D. Dolgos et al., "Full-band Monte Carlo simulation of high-energy carrier transport in single photon avalanche diodes," *J. Appl. Phys.*, vol. 110, no. 8, art. 084507, 2011.

[8] X. Zhou et al., "A simple Monte Carlo model for prediction of avalanche multiplication process in Silicon," *J. Instrum.*, vol. 7, art. P08006, 2012.

[9] E. Van Sieleghem et al., "A Near-Infrared Enhanced Silicon Single-Photon Avalanche Diode With a Spherically Uniform Electric Field Peak", *IEEE Electron Device Lett.*, vol. 42, no. 6, pp. 879–882, 2021.

[10] C. Jacoboni et al., "A review of some charge transport properties of silicon," *Solid State Electron.*, vol. 20, no. 2, pp. 77-89, 1977.

[11] M. Valdinoci et al., "Impact-ionization in silicon at large operating temperature," in *IEEE SISPAD*, pp. 27–30, 1999.